Theoretical Study on the Reaction of the Phenoxy Radical with O2, OH and NO2

ARTICLE *in* INTERNATIONAL JOURNAL OF QUANTUM CHEMISTRY · FEBRUARY 2012

Impact Factor: 1.43 · DOI: 10.1002/qua.23074

3 AUTHORS:

Marwan M. Batiha

19 PUBLICATIONS **52** CITATIONS

SEE PROFILE

Ala'a Al-Muhtaseb

Sultan Qaboos University

71 PUBLICATIONS **1,170** CITATIONS

SEE PROFILE

Mohammednoor Altarawneh

Murdoch University

81 PUBLICATIONS **524** CITATIONS

SEE PROFILE

Theoretical Study on the Reaction of the Phenoxy Radical with O_2, OH, and NO_2

MARWAN BATIHA, ALA'A H. AL-MUHTASEB, MOHAMMEDNOOR ALTARAWNEH

Faculty of Engineering, Department of Chemical Engineering, Al-Hussein Bin Talal University, Ma'an-Jordan

Received 29 September 2010; accepted 19 January 2011
Published online in Wiley Online Library (wileyonlinelibrary.com).
DOI 10.1002/qua.23074

ABSTRACT: Unlike the chemistry underlying the self-coupling of phenoxy (C_6H_5O) radicals, there are very limited kinetics data at elevated temperatures for the reaction of the phenoxy radical with other species. In this study, we investigate the addition reactions of O_2, OH, and NO_2 to the phenoxy radical. The formation of a phenoxy-peroxy is found to be very slow with a rate constant fitted to $k = 1.31 \times 10^{-20} T^{2.49} \exp(-9300/T)$ $cm^3/mol/s$ in the temperature range of (298–2,000 K) where the addition occurs predominantly at the *ortho* site. Our rate constant is in line with the consensus of opinions in the literature pointing to the observation of no discernible reaction between the oxygen molecule and the resonance-stabilized phenoxy radical. Addition of OH at the *ortho* and *para* sites of the phenoxy radical is found to afford adducts with sizable well depths of 59.8 and 56.0 kcal/mol, respectively. The phenoxy-NO_2 bonds are found to be among the weakest known phenoxy-radical bonds (1.7–8.7 kcal/mol). OH- and O_2-initiated mechanisms for the degradation of atmospheric phenoxy appear to be negligible and the fate of atmospheric phenoxy is found to be controlled by its reaction with NO_2. Int J Quantum Chem 000: 000–000, 2011

Key words: phenoxy radicals; O_2; OH; NO_2; rate constant; atmospheric life time; DFT

Introduction

Phenoxy radical is a key intermediate in the oxidation of benzene [1]. The most frequently proposed mechanism suggests that phenoxy radical is formed via the fission of the peroxyl bond in phenylperoxy at intermediate to high temperatures [2]. Phenoxy radical is also formed by attack of the O/H radical pool on the benzene ring. Other routes to the formation of the phenoxy radical involve the pyrolysis and oxidation of phenol [3] and anisole [4] through the direct homolysis of the O—H and O—CH_3 bond, respectively. The most important exit channel of the phenoxy radical is characterized by ring

Correspondence to: M. Altarawneh; e-mail: mn.Alt@ahu.edu.jo

Additional Supporting Information may be found in the online version of this article.

contraction/CO elimination. Also, phenoxy radical serves as a potent precursor for the homogenous formation for polychlorinated dibenzo-*p*-dioxins and furans (PCDD/F) and polychlorinated biphenyls (PCB) [5].

Phenoxy radical is regarded a persistent free environmental radical (PFR) [6]. Mounting evidence indicates that phenoxy radical resists decomposition by oxidation even at high temperatures [7]. This is primarily due to the resonance-stabilized structure of the phenoxy radical where the electronic charge is delocalized through the benzene ring as well as on the phenolic oxygen. Consensus of opinions in the literature points to the very low reactivity of the phenoxy radical with the oxygen molecule [7]. This low reactivity has encouraged researchers to re-consider the contribution of the gas-phase route for the formation of PCDD and PCB.

Although the chemistry underlying the self-condensation of the phenoxy radicals has been extensively studied, both experimentally [8] and theoretically [9], kinetics data concerning the association of the phenoxy radical with molecular oxygen or O/H radicals are rather scarce. This may be primarily due to the difficulty in finding a convenient source for the phenoxy radical under experimental conditions [10]. So far, efforts have focused on tracing the fate of atmospheric phenoxy through investigating reactions with the oxygen molecule and NO_x species at ambient conditions [10].

To this end, we report herein a theoretical investigation on reactions of the phenoxy radical with the oxygen molecule and the hydroxyl radical as the two most plausible bimolecular competing routes for the phenoxy radical under oxidative oxidations. Although the derivation of rate constants for these two reactions represents the core of this study, we also shed light on the most important atmospheric sink pathway for the phenoxy radical as a consequence of rate constants calculated in this study.

Computational Details

Optimized geometries and harmonic vibrational frequencies of all species and transition states were calculated using the density functional theory (DFT) of BB1K [11, 12] using the 6-311+G(d,p) basis set [13] as implemented in the Gaussian 03 [14] suite of programs. The BB1K functional is a meta hybrid DFT method that deploys an HF exchange fraction along with the abstraction of kinetic energy density from Kohn–Sham orbitals [15]. It has been found that BB1K considerably surpasses all hybrid DFT methods including B3LYP [16] in locating saddle-points and estimating their barrier heights.

The rate constants for OH and NO_2 addition to phenoxy were calculated using variational transition state theory (VTST) [17–21] in which the rate constant is minimized as a function of reaction coordinate (bond elongation) and temperature. Input structures to VTST were obtained by performing relaxed potential energy scans along the stretched phenoxy-OH and phenoxy-NO_2 bonds at 0.1–0.15 Å intervals. All transition state structures exhibit a single negative frequency associated with the fission of the phenoxy-OH and phenoxy-NO_2 bonds. Variational rate constants were initially obtained for the barrierless dissociation reactions of phenoxy-OH or phenoxy-NO_2 back into phenoxy and OH or NO_2. Calculated equilibrium constants were then used to estimate the variational forward association reactions according to the principle of microscopic reversibility. Note that phenoxy belongs to the C_{2V} point group, which results in doubling the forward association rate constants using this treatment. Conventional transition state theory (TST) is used to calculate rate constants for the oxygen molecule addition to phenoxy. All rate constants calculations are performed with the aid of "The Rate" code available online at the CSEO resource (http://www.cseo.net) [22].

Results and Discussion

REACTION OF PHENOXY RADICAL (C_6H_5O) WITH THE OXYGEN MOLECULE (O_2 $^3\Sigma G$)

Phenoxy radical contains two potential sites for addition of the triplet oxygen molecule, namely the *ortho* and *para* sites. The resultant two adducts, *o*-PhxOO and *p*-PhxOO, respectively, are shown in Figure 1. The formation of these two adducts is associated with endothermicities of 10.0 and 6.4 kcal/mol, respectively. The oxygen molecule encounters the transition structures TS1 and TS2 (Fig. 1) in its addition to form *o*-PhxOO or *p*-PhxOO. Barrier heights for these two transition states are very comparable and amount to

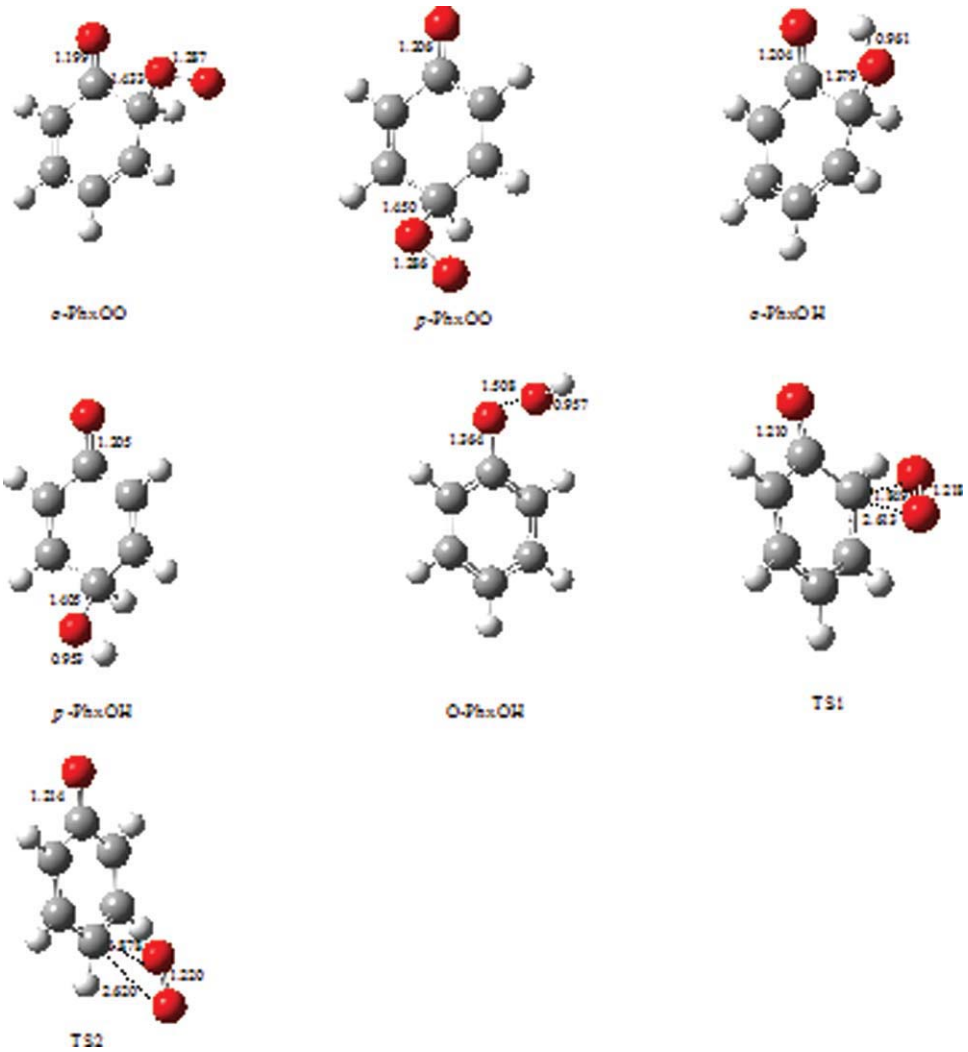

FIGURE 1. Optimized structures at the BB1K/6-311+G(d,p) level of theory for reactions involving O_2 and OH. Distances are in Å. [Color figure can be viewed in the online issue, which is available at wileyonlinelibrary.com.]

19.1 and 19.3 kcal/mol. Reaction energies and activation barriers calculated here are in close agreement with values obtained previously at various theoretical levels including BHandHLYP/6-31G(d) and B3LYP/6-31G(d,p) [23]. The located transition states are used to derive rate constants for oxygen molecule addition to phenoxy according to TST in which we have corrected for the tunneling effect using a one dimensional Eckart function [24]. The calculated modified Arrhenius rate parameters are given in Table I for the formation of the two isomers. From the derived rate constant, it is evident that the oxygen molecule preferentially adds at the *para* site.

In an experiment using a pulse radiolysis and FT-IR smog chamber, Platz et al. [25] obtained an upper limit of $\leq 5 \times 10^{-21}$ $cm^3/mol/s$ at 296 K for the title reaction. Also, Berho and Lesclaux [10] observed no discernible reaction between O_2 and phenoxy radicals for temperatures as high as 500 K whereby they assigned an upper limit of $\leq 2 \times 10^{-18}$ $cm^3/mol/s$. Our calculated rate constants amount to 5.9×10^{-18} and 2.5×10^{-21} $cm^3/mol/s$ at 500 and 296 K, respectively. Thus, our calculated rate constants are in satisfactory agreement with the very limited available literature data.

In kinetics models designed to describe the homogenous formation of PCDD/F from the self-coupling of phenoxy in the temperature range of 573–973 K, a value of 1.66×10^{-12} $cm^3/mol/s$ (10^{11} $cm^3/mol/s$) is often used for the phenoxy/O_2 reaction [7]. At a temperature of 700 K, our

TABLE I

Arrhenius rate parameters (A', n, E_a).

	A' (cm^3/mol/s)	n	E_a/R (K)
Phenoxy + OH →*o*-PhxOH (VTST)	5.25×10^{-11}	0.0	−1,300
Phenoxy + OH →*p*-PhxOH (VTST)	1.53×10^{-18}	2.27	−1,900
Phenoxy + OH →O-PhxOH (VTST)	6.88×10^{-14}	0.0	−5,400
Phenoxy + NO_2 →*o*-PhxNO_2 (VTST)	2.04×10^{-20}	1.83	−5,600
Phenoxy + NO_2 →*p*-PhxNO_2 (VTST)	2.78×10^{-15}	0.0	−4,600
Phenoxy + NO_2 →O-PhxNO_2 (VTST)	1.09×10^{-14}	0.0	−3,900
Phenoxy + O_2 →*o*-PhxOO (TST)	3.28×10^{-21}	2.41	9,200
Phenoxy + O_2 →*p*-PhxOO (TST)	1.31×10^{-20}	2.49	9,300

calculated rate constant merely approaches 1.98×10^{-16} cm^3/mol/s. This reveals that the consumption of the phenoxy radical by the oxygen molecule predicted herein is significantly lower than the commonly used estimate in kinetics models for the gaseous formation of PCDD/F from phenoxy.

To estimate the lifetime of the two phenoxy peroxy adducts, rate constant expressions for the unimolecular dissociation into phenoxy and oxygen molecule are fitted to modified Arrhenius parameter as:

$$k(o\text{−PHxOO} \rightarrow \text{Phenoxy} + O_2)\ \ 3.8 \times 10^{11} T^{0.37} \exp(-4600/T)\ \text{s}^{-1}$$

$$k(p - \text{PHxOO} \rightarrow \text{Phenoxy} + O_2)\ \ 3.6 \times 10^{11} T^{0.38} \exp(-6090/T)\ \text{s}^{-1}$$

Lifetimes (τ) of the two phenoxy peroxyl adducts are determined as $2\ln(2)/k$ and are given in Figure 2 as function in temperatures. At 298.15, lifetimes of *o*-PhxOO and *p*-PhxOO conditions amounts to 2.2×10^{-6} s and 2.9×10^{-4} s; respectively. This indicates that even at normal atmospheric conditions, the phenoxy peroxyl adducts are short-lived and their fate is the dissociation back into phenoxy and oxygen molecule. As shown in Figure 2, lifetime decreases exponentially with increase in temperature. At temperatures relevant to the homogenous formation of dioxins, that is, 450°C to 600°C [7]; both phenoxy peroxyl adducts are predicted to be very short-lived species, in agreement with the consensus opinions in literature pointing to the negligible oxidative decomposition of phenoxy at elevated temperatures, which in turns enable it undergoing self-dimerization to produce dioxins.

REACTION OF THE PHENOXY RADICAL WITH THE HYDROXYL RADICAL

Hydroxyl radical (OH) addition to the resonance stabilized structure of the phenoxy radical affords three distinct isomers characterizing addition at the *ortho*, *para,* and the phenolic O sites, respectively. Optimized structures for the three adducts formed, viz., *o*-PhxOH, *p*-PhxOH, and O-PhxOH are given in Figure 1. Potential energy surface (PES) for the hydroxyl addition is given in Figure 2.

o-PhxOH and *p*-PhxOH are found to be in appreciable enthalpy well depths of −59.8 and −56.0 kcal/mol, respectively, with respect to the separated reactants. Formation of the O-PhxOH adduct is linked with a trivial exothermicity of 2.3 kcal/mol. The slight exothermicity associated with the formation of O-PhxOH in comparison with the significant exothermicity for the formation of *o*-PhxOH and *p*-PhxOH is due to the

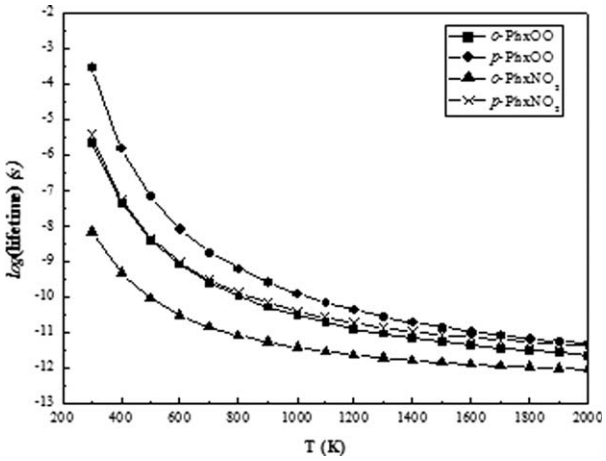

FIGURE 2. Estimated life time.

thermodynamically unfavorable coupling of the negatively charged phenolic oxygen and the hydroxyl O. Bond enthalpies of dissociation of OH-phenoxy adducts is compared here with the corresponding enthalpies of dissociation in other resonance stabilized radicals. Bond dissociation enthalpies of OH-cyclohexadienyl and *o*-OH-1,4-pentadien-3yl are estimated to be 62.8 kcal/mol and 60.9 kcal/mol, that is, in close agreement with the corresponding calculated value for *o*-PhxOH (58.7 kcal/mol). This indicates that the three considered resonance stabilized radicals has very similar tendency toward resonance aromatization.

As a typical radical–radical recombination, no discrete transition structure could be located for any of these addition processes. To provide reaction rate constants for the reaction of the phenoxy radical with the hydroxyl radical, VTST is deployed. The general procedure used here has been successfully applied to derive rate constants for phenoxy + H [26], 2-chlorophenoxy + H [27], and phenoxy + NO [28].

The potential energy surface (PES) for the addition reaction is mapped out by performing partial optimization for the phenoxy + OH system in which the phenoxy $\cdots$ OH distance is fixed at intervals of 0.1 Å while allowing the remaining coordinates to fully relax at the BB1K/6-311+G(d,p) level of theory. As the association involves two free radicals, electronic energies for the minimum energy points (MEP) along the specified PES are not accurate due to the multireference character (MRC) which the system exhibits when intersystem-crossing between singlet and triplet states takes place. To surmount this problem, energies for the bond fission of phenoxy $\cdots$ OH at the MEP were represented by the Morse function:

$$V(r) = D_e\{1 - \exp -[\beta(r - r_e)]\}^2$$

where r_e is the equilibrium phenoxy-OH distance in each of the three PhxOH adducts, r is the stretched phenoxy $\cdots$ OH distance, D_e is the electronic bond energy of phenoxy $\cdots$ OH (without zero point energy correction), and β equals $(k_e/2D_e)^{1/2}$ where k_e is the force constant corresponding to the vibrational frequency associated with the stretch of the phenoxy $\cdots$ OH bond in the three PhxOH adducts. For example, for the *p*-PhxOH adduct, we have obtained D_e = 60.3 kcal/mol, β = 1.74 Å^{-1}, and r_e = 1.405 Å at the BB1K/6-311+G(d,p) level of theory.

Variational rate constants were calculated as a function of the phenoxy $\cdots$ OH bond elongation and temperature for each of the three PhxOH adducts. Rate constants for the association reaction leading to the formation of *o*-PhxOH are given in Table II. The minimum rate constants labeling the position of the transition structure at each temperature are highlighted. Rate constants for the other two PhxOH adducts are given in the Supporting Information.

The association reaction for the formation of the *o*-PhxOH adduct is found to be controlled by a very loose 3.30 Å transition structure in the temperature window of 298–900 K, tightening somewhat to 3.20 Å at higher temperatures. In view of the mounting exothermic nature of the hydroxyl addition affording the moiety of *o*-PhxOH, a very loose transition structure is not an unexpected occurrence. The behavior of the *p*-PhxOH system obeys to a large extent the general features of the *o*-PhxOH system discussed above. In contrast, the formation of O-PhxOH is characterized by a somewhat tight transition structure in the range of 2.10–2.20 Å. The variational rate constants for the three adducts have been fitted to Arrhenius parameters as given in Table I. To the best of our knowledge, the data presented herein are the first estimates for the reaction rate constant for hydroxyl addition to the phenoxy radical.

Because of the very shallow well depth of the O-PhxOH in reference to the separated reactants (2.3 kcal/mol), the most likely exit channel for this adduct is assumed to be the dissociation back to OH and phenoxy. In an analogy with cyclohexadienone [29], the most likely decomposition route for *o*- and *p*-PhxOH is expected to be via β C—C bond scission.

REACTION OF PHENOXY RADICAL WITH NO_2

Potential energy surface for the reaction of NO_2 with the phenoxy radical is mapped out in Figure 3 on the singlet surface. Geometries of transition structures and products are given in Figure 4. As shown in Figure 3, addition of NO_2 to the phenoxy radical can occurs via the O or N sites in NO_2. Addition of NO_2 through it's N atom affords the structures *o*-PhxNO$_2$, *p*-PhxNO$_2$, and O-PhxNO$_2$. The formation of these three structures is slightly exothermic by 5.3, 8.7, and 1.7 kcal/mol. Thus, addition at the *para* site is preferred. Addition of NO_2 through one of its

TABLE II

Rate constants (k, cm^3/mol/s) as a function of temperature and position for the barrierless reaction of phenoxy + OH → *o*-PhxOH.

Temperature (K)	Distance (Å)			
	3.1	3.2	3.3	3.4
298.15	2.31×10^{-7}	2.37×10^{-8}	$\mathbf{5.93 \times 10^{-9}}$	1.21×10^{-9}
400	1.57×10^{-8}	2.84×10^{-9}	$\mathbf{1.17 \times 10^{-9}}$	3.78×10^{-10}
500	3.48×10^{-9}	8.89×10^{-10}	$\mathbf{4.96 \times 10^{-10}}$	2.11×10^{-10}
600	1.38×10^{-9}	4.43×10^{-10}	$\mathbf{3.02 \times 10^{-10}}$	1.54×10^{-10}
700	7.53×10^{-10}	2.84×10^{-10}	$\mathbf{2.24 \times 10^{-10}}$	1.30×10^{-10}
800	4.98×10^{-10}	2.12×10^{-10}	$\mathbf{1.87 \times 10^{-10}}$	1.20×10^{-10}
900	3.73×10^{-10}	1.75×10^{-10}	$\mathbf{1.67 \times 10^{-10}}$	1.16×10^{-10}
1,000	3.04×10^{-10}	$\mathbf{1.54 \times 10^{-10}}$	1.57×10^{-10}	1.16×10^{-10}
1,100	2.63×10^{-10}	$\mathbf{1.41 \times 10^{-10}}$	1.53×10^{-10}	1.18×10^{-10}
1,200	2.37×10^{-10}	$\mathbf{1.34 \times 10^{-10}}$	1.52×10^{-10}	1.22×10^{-10}
1,300	2.20×10^{-10}	$\mathbf{1.30 \times 10^{-10}}$	1.53×10^{-10}	1.28×10^{-10}
1,400	2.10×10^{-10}	$\mathbf{1.29 \times 10^{-10}}$	1.57×10^{-10}	1.35×10^{-10}
1,500	2.03×10^{-10}	$\mathbf{1.29 \times 10^{-10}}$	1.61×10^{-10}	1.43×10^{-10}
1,600	2.00×10^{-10}	$\mathbf{1.30 \times 10^{-10}}$	1.67×10^{-10}	1.51×10^{-10}
1,700	1.99×10^{-10}	$\mathbf{1.33 \times 10^{-10}}$	1.74×10^{-10}	1.61×10^{-10}
1,800	2.00×10^{-10}	$\mathbf{1.36 \times 10^{-10}}$	1.82×10^{-10}	1.71×10^{-10}
1,900	2.01×10^{-10}	$\mathbf{1.40 \times 10^{-10}}$	1.91×10^{-10}	1.83×10^{-10}
2,000	2.05×10^{-10}	$\mathbf{1.45 \times 10^{-10}}$	2.01×10^{-10}	1.94×10^{-10}

two O atoms produces *o*-PhxONO and *p*-PhxONO moieties. The formation of these two adducts are slightly endoergic by 5.7 and 6.8 Kcal/mol, respectively. Further transformation of *o*-PhxONO and *p*-PhxONO is considered. Direct fission of the O-NO bond requires 32.1 and 31.2 for *o*-PhxONO and *p*-PhxONO adducts, respectively, which results in the formation of the alkoxy quinone-type radicals; M1 and M2.

Alternatively, two epoxy-type radical (M3 and M4) could be produced via the transition structures TS3 and TS4, which resides 38.5 and 45.7 kcal/mol, respectively, above the initial entrance channel. As shown in Figure 3, the formation of M3 and M4 is associated with endoergicity of 22.0 and 12.4 kcal/mol, respectively, with respect to the entrance channel.

Concentric movement of H gem to C atom in *o*-PhxONO and *p*-PhxONO and the departure of NO through TS5 and TS6 results in the formation of the two semi-quinone-type radicals; M5 and M6. Formation of M5 and M6 is predicted to be exoergic by 21.7 kcal/mol and 27.8 kcal/mol, respectively, with respect to the entrance channel whereas TS5 and TS6 resides 48.3 kcal/mol and 43.3 kcal/mol, respectively, above the entrance channel.

For the *o*-PhxNO$_2$, *o*-PhxNO$_2$, and O PhxNO$_2$ adducts, the MEP is approximated by a Morse potential. For example, Morse parameters calculated for the fitting of the PES of the NO$_2$ addition to phenoxy to produce the *p*-PhxNO$_2$ adduct are $D_e = 12.9$ kcal/mol, $\beta = 4.19$ Å^{-1}, and $r_e = 1.519$ Å at the BB1K/6-311+G(d,p) level of theory. For the *p*-PhxNO$_2$ adduct, the rate constants from each contributing transition state structure are given in Table III and the variational rate constant

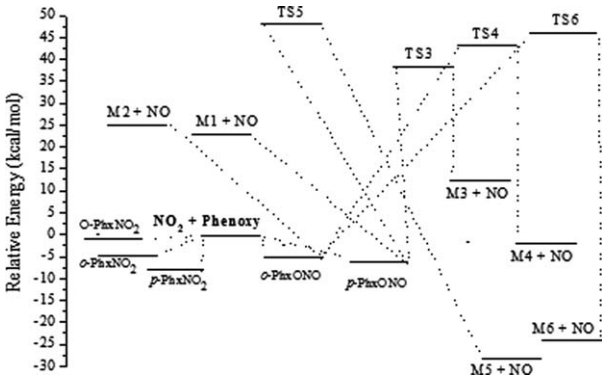

FIGURE 3. Potential energy surface for NO$_2$ addition to phenoxy.

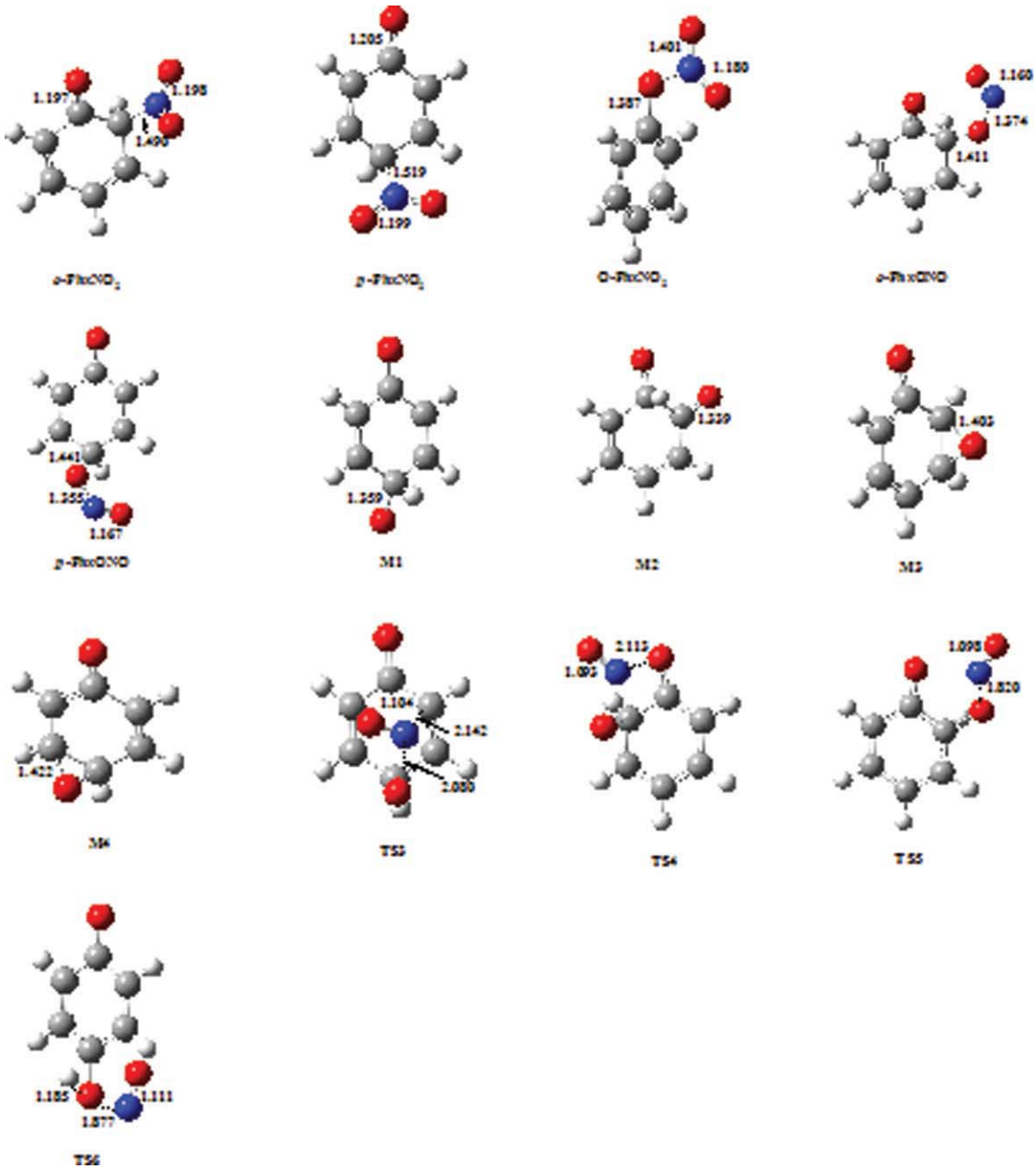

FIGURE 4. Optimized structures at the BB1K/6-311+G(d,p) level of theory for reactions involving NO_2. Distances are in Å. [Color figure can be viewed in the online issue, which is available at wileyonlinelibrary.com.]

is highlighted where the position of the transition structure is within a bond elongation of [2.22–2.27 Å]. Variational rate constants for the formation of the *o*-$PhxNO_2$ and O-$PhxNO_2$ adducts are given in the Supporting Information. The variational rate constants obtained for the three adducts are fitted to Arrhenius parameters in Table I. In the view of the very similar reaction energies for the formation of *o*-PhxONO and *p*-PhxONO with that of *o*-$PhxNO_2$, it can be assumed that the formation of *o*-PhxONO and *p*-PhxONO proceed in a very similar rate with that of *o*-$PhxNO_2$.

As shown in Figure 3, the most accessible exit channel for the $PhxNO_2$ adducts are dissociation back into NO_2 and phenoxy. Thus, the lifetime of the five initial $PhxNO_2$ adducts can be measured

TABLE III

Rate constants (k, cm^3/mol/s) as a function of temperature and position for the barrierless reaction of phenoxy + NO_2 → p-$PhxNO_2$.

	Distance (Å)					
Temperature (K)	1.97	2.12	2.22	2.27	2.37	2.42
298.15	2.08×10^{-6}	3.62×10^{-7}	2.39×10^{-8}	$\mathbf{1.90 \times 10^{-8}}$	1.94×10^{-8}	1.08×10^{-7}
400	1.47×10^{-8}	4.82×10^{-9}	3.02×10^{-10}	$\mathbf{2.63 \times 10^{-10}}$	3.00×10^{-10}	2.41×10^{-9}
500	8.51×10^{-10}	4.09×10^{-10}	2.38×10^{-11}	$\mathbf{2.18 \times 10^{-11}}$	2.68×10^{-11}	2.80×10^{-10}
600	1.38×10^{-10}	8.59×10^{-11}	4.60×10^{-12}	$\mathbf{4.38 \times 10^{-12}}$	5.66×10^{-12}	7.30×10^{-11}
700	4.00×10^{-11}	3.00×10^{-11}	1.48×10^{-12}	$\mathbf{1.45 \times 10^{-12}}$	1.94×10^{-12}	2.98×10^{-11}
800	1.65×10^{-11}	1.43×10^{-11}	6.52×10^{-13}	$\mathbf{6.52 \times 10^{-13}}$	8.98×10^{-13}	1.60×10^{-11}
900	8.62×10^{-12}	8.33×10^{-12}	$\mathbf{3.53 \times 10^{-13}}$	3.59×10^{-13}	5.06×10^{-13}	1.02×10^{-11}
1,000	5.28×10^{-12}	5.57×10^{-12}	$\mathbf{2.20 \times 10^{-13}}$	2.27×10^{-13}	3.26×10^{-13}	7.39×10^{-12}
1,100	3.63×10^{-12}	4.12×10^{-12}	$\mathbf{1.52 \times 10^{-13}}$	1.58×10^{-13}	2.31×10^{-13}	5.81×10^{-12}
1,200	2.71×10^{-12}	3.26×10^{-12}	$\mathbf{1.13 \times 10^{-13}}$	1.19×10^{-13}	1.76×10^{-13}	4.86×10^{-12}
1,300	2.15×10^{-12}	2.73×10^{-12}	$\mathbf{8.95 \times 10^{-14}}$	9.47×10^{-14}	1.41×10^{-13}	4.25×10^{-12}
1,400	1.80×10^{-12}	2.38×10^{-12}	$\mathbf{7.38 \times 10^{-14}}$	7.86×10^{-14}	1.18×10^{-13}	3.85×10^{-12}
1,500	1.56×10^{-12}	2.15×10^{-12}	$\mathbf{6.30 \times 10^{-14}}$	6.75×10^{-14}	1.03×10^{-13}	3.59×10^{-12}
1,600	1.39×10^{-12}	1.98×10^{-12}	$\mathbf{5.53 \times 10^{-14}}$	5.95×10^{-14}	9.11×10^{-14}	3.41×10^{-12}
1,700	1.27×10^{-12}	1.87×10^{-12}	$\mathbf{4.96 \times 10^{-14}}$	5.36×10^{-14}	8.26×10^{-14}	3.30×10^{-12}
1,800	1.18×10^{-12}	1.79×10^{-12}	$\mathbf{4.53 \times 10^{-14}}$	4.92×10^{-14}	7.63×10^{-14}	3.23×10^{-12}
1,900	1.12×10^{-12}	1.73×10^{-12}	$\mathbf{4.20 \times 10^{-14}}$	4.58×10^{-14}	7.14×10^{-14}	3.20×10^{-12}
2,000	1.08×10^{-12}	1.70×10^{-12}	$\mathbf{3.95 \times 10^{-14}}$	4.32×10^{-14}	6.76×10^{-14}	3.19×10^{-12}

by considering the reverse reaction rate constant. As illustrative cases, the reverse reaction rate constants for the formation of o-$PhxNO_2$ and p-$PhxNO_2$ are fitted to modified Arrhenius parameters as:

$$k(o\text{-}\mathrm{PHxNO_2} \rightarrow \mathrm{Phenoxy} + \mathrm{NO_2})\ \ 3.9 \times 10^{14} T^{-0.5} \exp(-3500/T)\ \mathrm{s}^{-1}$$

$$k(p\text{-}\mathrm{PHxNO_2} \rightarrow \mathrm{Phenoxy} + \mathrm{NO_2})\ \ 2.7 \times 10^{11} T^{-0.6} \exp(-5200/T)\ \mathrm{s}^{-1}$$

Because of the shallow well-depth of the five considered $PhxNO_2$ adducts, they all have very short life time even at low temperatures. For instant, lifetime of o-$PhxNO_2$ and p-$PhxNO_2$ are found to amount to 2.7×10^{-9} and 7.2×10^{-9} s, respectively, at 298.15 K.

ATMOSPHERIC IMPLICATIONS

The atmospheric fate of the phenoxy radical was investigated extensively by Platz et al. [25]. The potential major sinks for the atmospheric phenoxy are considered to be its reactions with NO, NO_2, and O_2. The reaction with O_2 was found to be too slow to compete with the reactions of NO and NO_2. The experimental results of Platz et al. imply that the removal of atmospheric phenoxy is controlled by reactions with NO_x species even in low polluted urban areas. Consumption by the hydroxyl group was not included. As the hydroxyl radical is the sole initiator for oxidative decomposition of hydrocarbons in the atmosphere [30], it is very informative to consider its role when attempting to investigate the contribution of each plausible decomposition channel. In this section, the reaction of NO_2 with phenoxy is considered to compare with the other two consumption rates involving the oxygen molecule and hydroxyl radical.

The atmospheric fate of the phenoxy radical was investigated extensively by Platz et al. [25]. The potential major sinks for the atmospheric phenoxy are considered to be its reactions with NO, NO_2, and O_2. The reaction with O_2 was found to be too slow to compete with the reactions of NO and NO_2. The experimental results of Platz et al. imply that the removal of atmospheric phenoxy is controlled by reactions with NO_x species even in low polluted urban areas. Consumption by the hydroxyl group was not included. As the hydroxyl radical is the sole

initiator for oxidative decomposition of hydrocarbons in the atmosphere [30], it is very informative to consider its role when attempting to investigate the contribution of each plausible decomposition channel.

To compare the three potential consumption routes, namely by O_2, OH, and NO_2, the overall rate constants (i.e., summation of the rate constants for the three isomers) for addition of each species are multiplied by the 12 h diurnal average concentration of each species. Concentrations of 5.17×10^{18}, 9.70×10^{5}, and 8.5×10^{11} mol/cm^3, respectively, are used for O_2, OH, and NO_2 (a typical figure for non-polluted areas), respectively [31], at 298.15 K, the calculated rates of consumption of phenoxy radical by O_2, OH, and NO_2, respectively, are estimated to be 4.29×10^{-9}, 5.98×10^{-3}, and 1.13×10^{5} s^{-1}. Accordingly, the atmospheric degradation of the phenoxy radical is most likely to proceed in an NO_2-initated mechanism and the roles of triplet oxygen molecule and hydroxyl in the consumption of atmospheric phenoxy appear to be very minor in comparison with the contribution of the NOx species. Thus, even with the inclusion of the hydroxyl radical, the fate of the phenoxy radical is dominated by its reaction with NO_x species in accord with the experimental findings of Platz et al. [25]. However, according to the estimated lifetimes, PhxOO adducts are expected to live longer than $PhxNO_2$ adducts at the atmospheric temperature. Nevertheless, the subsequent degradation mechanism involves continuing addition of oxygen molecule to the initial adducts.

Conclusions

Reaction rate constants are theoretically derived for the additions of O_2, OH, and NO_2 to the phenoxy radical. Oxygen and hydroxyl addition at the *ortho* sites of the phenoxy radical dominates additions over the *para* and the phenolic oxygen sites. Because of the resonance stabilized structure of phenoxy, these additions are found to be very slow in accord with the experimental observations. The calculated rate constants at 298.15 for the consumption of the phenoxy radical by the predominant NO_2 route yield a lifetime of 0.34 day for atmospheric phenoxy.

ACKNOWLEDGMENT

The authors acknowledge access to the computing facilities at the Australian Centre of Advanced Computing and Communications (ac3).

References

1. Alzueta, M. U.; Oliva, M.; Glarborg, P. Int J Chem Kinet 2000, 32, 498.
2. Carpenter, B. K. J Am Chem Soc 1993, 115, 9806.
3. Brezinsky, K.; Pecullan, M.; Glassman, I. J Phys Chem A 1998, 102, 8614.
4. Pecullan, M.; Brezinsky, K.; Glassman, I. J Phys Chem A 1997, 101, 3305.
5. Altarawneh, M.; Dlugogorski, B. Z.; Kennedy, E. M.; Mackie, J. C. J Phys Chem A 2007, 111, 2563.
6. Maskos, Z.; Dellinger, B. Energy Fuels 2008, 22, 1675.
7. Altarawneh, M.; Dlugogorski, B. Z.; Kennedy, E. M.; Mackie, J. C. Prog Energy Combust Sci 2009, 35, 245.
8. Mulholland, J. A.; Akki, U.; Yang, Y.; Ryu, J. Y. Chemosphere 2001, 42, 719.
9. Asatryan, R.; Khachatryan, L.; Dellinger, B. J Phys Chem A 2005, 109, 11198.
10. Berho, F.; Lesclaux, R. Chem Phys Lett 1997, 279, 289.
11. Zhao, Y.; Gonzalez-Garcia, N.; Truhlar, D. G. J Phys Chem A 2005, 109, 2012.
12. Zhao, Y.; Lynch, B. J.; Truhlar, D. G. J Phys Chem A 2004, 108, 2715.
13. Montgomery, J. A.; Ochterski, J. W.; Petersson, G. A. J Chem Phys 1994, 101, 5900.
14. Frisch, M. J.; Trucks, G. W.; Schlegel, H. B.; Scuseria, G. E.; Robb, M. A.; Cheeseman, J. R.; Zakrzewski, V. G.; Montgomery, J. A.; Stratmann, R. E.; Burant, J. C.; Dapprich, S.; Millam, J. M.; Daniels, R. E.; Kudin, K. N.; Strain, M. C.; Farkas, O.; Tomasi, J.; Barone, V.; Cammi, M.; Mennucci, R.; Pomelli, B.; Adamo, C.; Clifford, C.; Ochterski, S.; Petersson, J.; Ayala, G. A.; Cui, P. Y.; Morokuma, Q.; Salvador, K.; Dannenberg, P.; Malick, J. J.; Rabuck, D. K.; Raghavachari, A. D.; Foresman, K.; JO Cioslowski, J. B.; Baboul, J. V.; Stefanov, A. G.; Liu, B. B.; Liashenko, G.; Piskorz, A.; Komaromi, P.; Gomperts, I.; Martin, R.; Fox, R. L.; Keith, D. J.; Al-Laham, T.; Peng, M. A.; Nanayakkara, C. Y.; Challacombe, A.; Gill, M.; Johnson, P. M. W.; Chen, B.; Wong, W.; Andres, M. W.; Gonzalez, J. L.; Head-Gordon, C. M.; Replogle, M.; Pople, E. S. Gaussian 03; Gaussian, Inc.; Pittsburgh, PA, 2001.
15. Kohn, W.; Sham, L. J Phys Rev A 1965, 140, 1133.
16. Becke, A. D. J Chem Phys 1996, 104, 1040.
17. Truhlar, D. G.; Isaacson, A. D.; Garrett, B. C. In Theory of Chemical Reaction Dynamics; Baer, M., Ed.; CRC Press: Boca Raton, FL, 1985; p 65.

18. Truong, T. N.; Truhlar, D. G. J Chem Phys 1990, 93, 1761.
19. Fast, P. L.; Truhlar, D. G. J Chem Phys 1998, 109, 3721.
20. Pu, J.; Truhlar, D. G. J Chem Phys 2002, 117, 1479.
21. Allison, C.; Truhlar, D. G. Modern Methods for Multidimensional Dynamics Computations in Chemistry; World Scientific: Singapore, 1998.
22. Duncan, W. T.; Bell, R. L.; Truong, T. N. J Comput Chem 1998, 19, 1039.
23. McFerrin, C. A.; Hall, R. W.; Dellinger, B. J Mol Struct 2008, 848, 16.
24. Eckart, C. Phys Rev 1930, 35, 1303.
25. Platz, J.; Nielsen, O. J.; Wallington, T. J.; Ball, J. C.; Hurley, M. D.; Straccia, A. M.; Schneider, W. F.; Sehested, J. J Phys Chem 1998, 102A, 7964.
26. Xu, Z. F.; Lin, M. C. J Phys Chem 2006, 110A, 1672.
27. Altarawneh, M.; Dlugogorski, B. Z.; Kennedy, E. M.; Mackie, J. C. J Phys Chem 2008, 112A, 3680.
28. Xu, S.; Lin, M. C. J Phys Chem 2005, 109B, 8367.
29. Zhu, L.; Bozzelli, J. W. J Phys Chem 2003, 107A, 3696.
30. Atkinson, R.; Baulch, D. L.; Cox, R. A.; Hampson, R. F.; Jr, N.; Troe, J. J Phys Chem Ref Data 1992, 21, 1125.
31. Atkinson, R.; Baulch, D. L.; Cox, R. A.; Hampson, R. F.; Jr, N.; Troe, J. J Phys Chem Ref Data 1989, 18, 881.